Chapter 5

Moho depths and crustal v_p/v_s ratios

5.1 Nature of the Moho

In the Earth's crust, *P* wave velocities are approx. 6 to 7 km/s. Below the Mohorovičić discontinuity (Moho), the *P* wave velocity abruptly increases to 8 km/s, which is an indication for a very sharp boundary between crustal rocks (in continental crust mainly granitic rocks and gabbro) and mantle rocks (peridotite). The Moho comprises major changes in chemical, rheological and seismic properties of the rocks. It was discovered by Andrija Mohorovičić in 1909 (*Mohorovičić*, 1910). Underneath continents, the Moho is usually between 30 and 50 km deep. The depth of Moho is an important parameter to characterize the overall structure of the crust and can often be related to geology and tectonic evolution of the region.

5.2 Data examples

Figure 5.1 shows data examples of *P* receiver functions recorded at stations near the intersection area of Eger Rift and Regensburg-Leipzig-Rostock zone (stations NALB, B24, NKC) as well as in the Saxothuringian unit (station BG07), Teplá-Barrandian (station B09) and Moldanubian unit (station B12/BM12). A strong positive signal is visible in the data of all stations at 3.0 to 4.5 s delay time, which is interpreted as the *P*-to-*S* converted signal from the Moho discontinuitiy. Accordingly, the positive signal at 11 to 13 s delay time and the negative signal at 15 to 17 s are interpreted as multiple reverberations within the crust (phases *PpPs* and *PsPs*+*PpSs*, respectively).

5.3 Observations

5.3.1 *Ps* delay times of the Moho discontinuity

The delay time of the *P*-to-*S* converted phase of the Moho discontinuity was read from the sum trace of each station of the BOHEMA passive seismic experiment (Figures 5.2 and 5.3). The obtained delay times vary between 3.0 and 4.5. The Moho delay times are displayed together with the piercing points of the individual rays at an interface at 30 km

depth to visualize where the obtained information originates. The piercing points have a horizontal distance to the recording station of 5-10 km.

The obtained delay times of the Moho *Ps* conversion reveal rather clear structures:

- In the Saxothuringian unit, delay times vary between 3.3 and 4.1 s. However, the majority of stations shows values around 3.5 to 3.6 s.
- In the Teplá-Barrandian unit, values increase from 3.4 s in the NW to 4.1 s in the SE.
- Beneath the western Eger Rift, delay time values clearly decrease up to approx. 3.0 s as was already indicated by *Geissler et al.* (2005).
- In the Moldanubian unit between the Central Bohemian and Bavarian Shear Zone, the delay time strongly increases to values of 4.3 to 4.5 s.

Along the Eger Rift towards ENE, unfortunately there is not enough data to investigate crustal thickness beneath the rift. However, the existing sparse data shows that there are no indications for an anomaly along the Eger Rift comparable to the delay time anomaly beneath the westernmost part of the rift.

Figure 5.1 a to f (next pages): *P* receiver functions recorded at temporary and permanent stations of the BOHEMA network. On the left of each figure, individual receiver functions are displayed in the time domain. The time axis shows the delay time of the *P*-to-*S* converted phases with respect to the *P* onset (time=0). The single traces are sorted according to their back azimuths, the latter of which are shown in the right box of each figure by red squares. Furthermore, the box on the right gives the epicentral distance of the corresponding event. The individual traces are filtered between 1 and 12 s and corrected for distance moveout for a reference epicentral distance of 67°. On top of the individual traces, the summation trace is shown.

a) Temporary station NALB (21 traces). Delay time of the Moho *Ps* conversion in the sum trace is 3.4 s, crustal multiples follow at 11.4 and 14.9 s. At 5.7 s appears a positive phase and at 7.3 s a strong negative phase which will be discussed in more detail in Chapter 6.2. In the individual traces, the amplitude of the converted signals varies strongly.
b) Temporary station B24 (15 traces). Delay time of the Moho *Ps* conversion in the sum trace is 3.2 s, crustal multiples follow at 12.6 and 15.5 s. Like at station NALB, at 5.7 s appears a positive phase and at 7.2 s a strong negative phase which will be discussed in more detail in Chapter 6.2.
c) Permanent station NKC (121 traces). Delay time of the Moho *Ps* conversion in the sum trace is 3.4 s, crustal multiples follow at 12.4 and 15.6 s. A positive signal after the Moho signal like at stations NALB and B24 is visible for eastern and western back azimuths, but not in the summation trace.
d) Temporary station BG07 (31 traces). Delay time of the Moho *Ps* conversion in the sum trace is 3.6 s, crustal multiples follow at 12.8 and 16.0 s. A positive and negative signal after the Moho signal also exist at 7.6 and 9.2 s, respectively, which is approximately 2 s later than at stations NALB and B24 (see a and b above).
e) Temporary station B09 (83 traces). Delay time of the Moho *Ps* conversion in the sum trace is 3.6 s, crustal multiples follow at 12.8 and 16.5 s.
f) Temporary station B12/BM12 (20 traces). Delay time of the Moho *Ps* conversion in the sum trace is 4.4 s, crustal multiples follow at 15.2 and 19.2 s.

a)

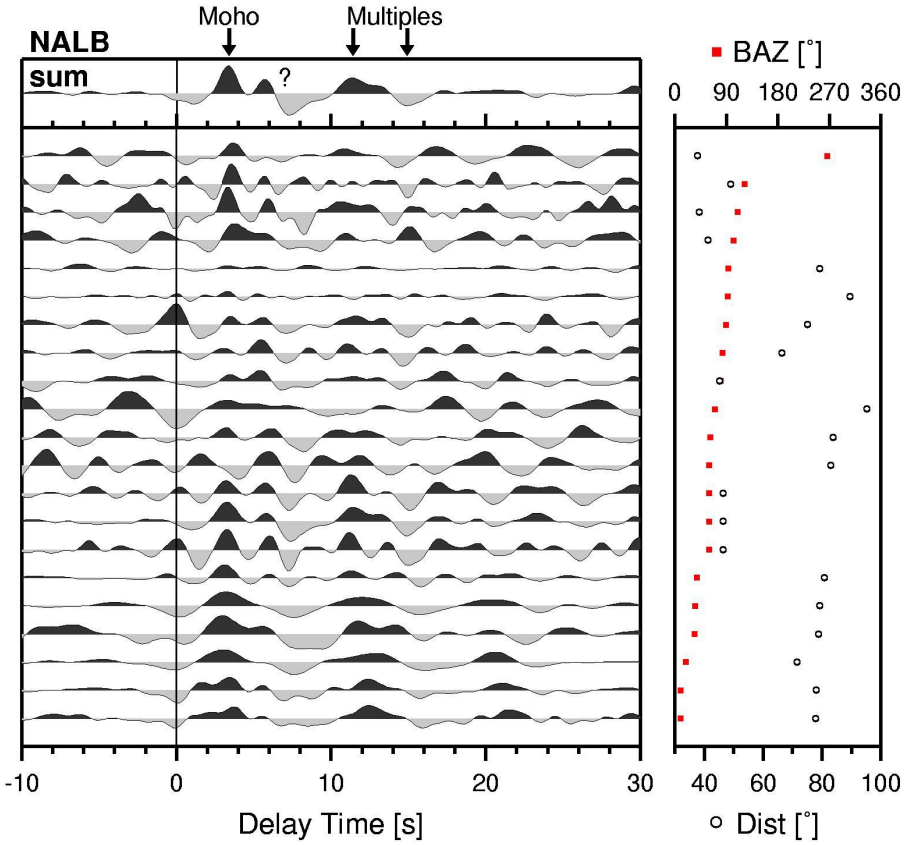
Moho
Multiples
NALB
sum
?
BAZ [°]
0 90 180 270 360
-10 0 10 20 30
Delay Time [s]
40 60 80 100
Dist [°]

b)

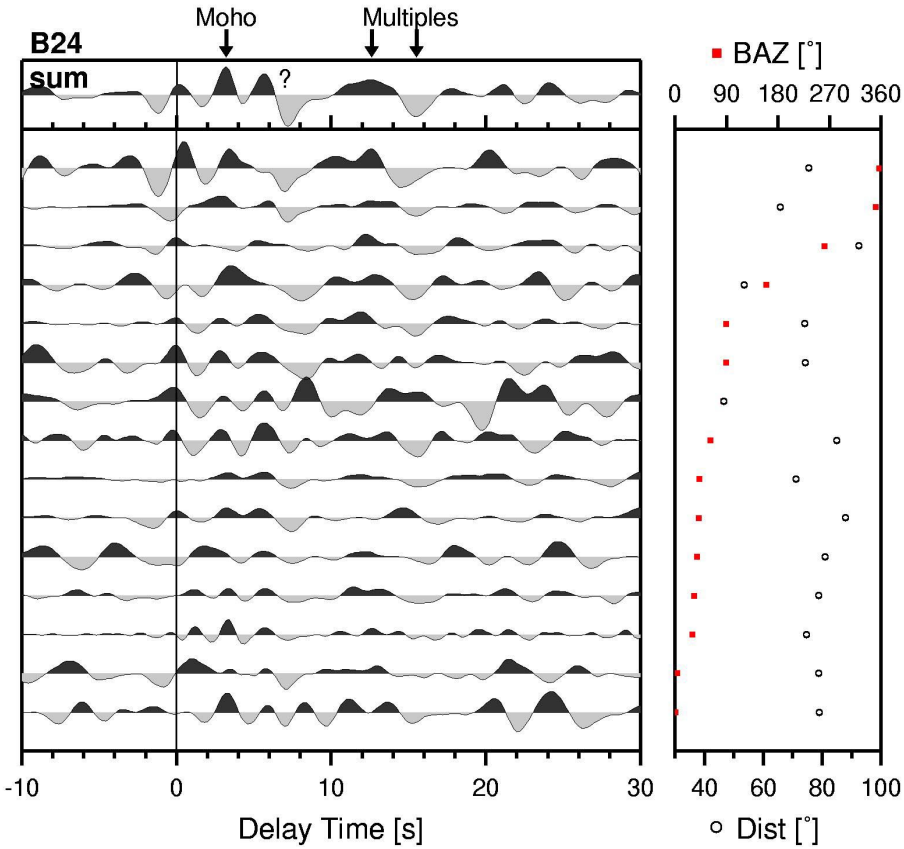
Moho
Multiples
B24
sum
?
BAZ [°]
0 90 180 270 360
-10 0 10 20 30
Delay Time [s]
40 60 80 100
Dist [°]

c)

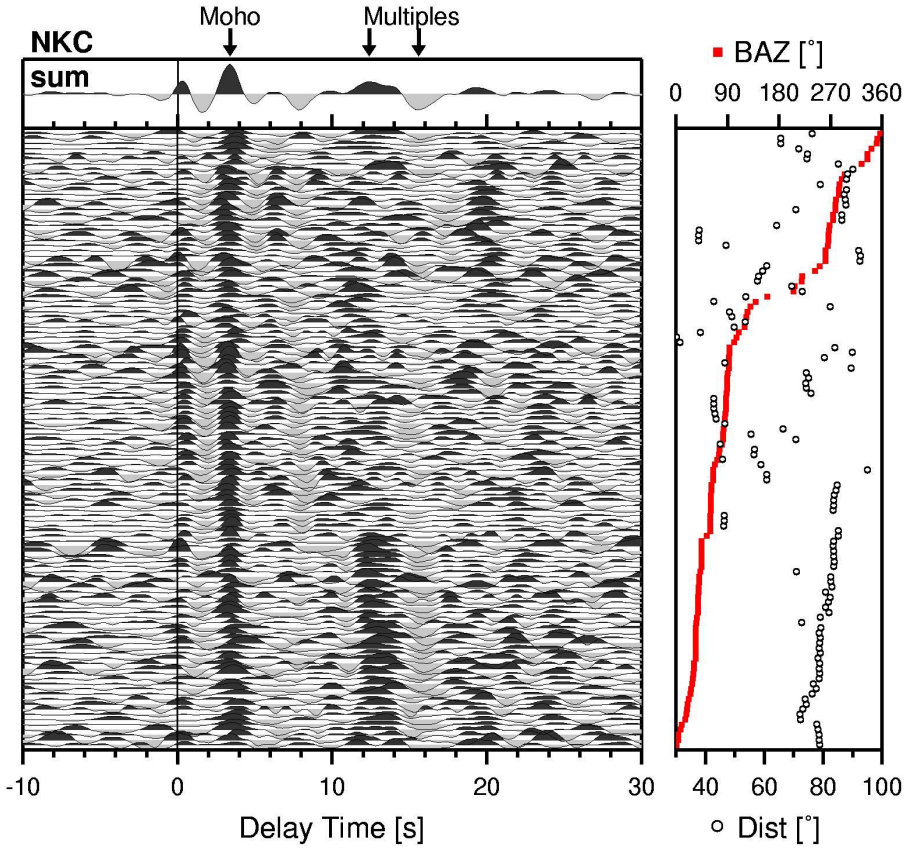
Moho
Multiples
NKC
sum
BAZ [°]
0 90 180 270 360
-10 0 10 20 30
Delay Time [s]
40 60 80 100
Dist [°]

d)

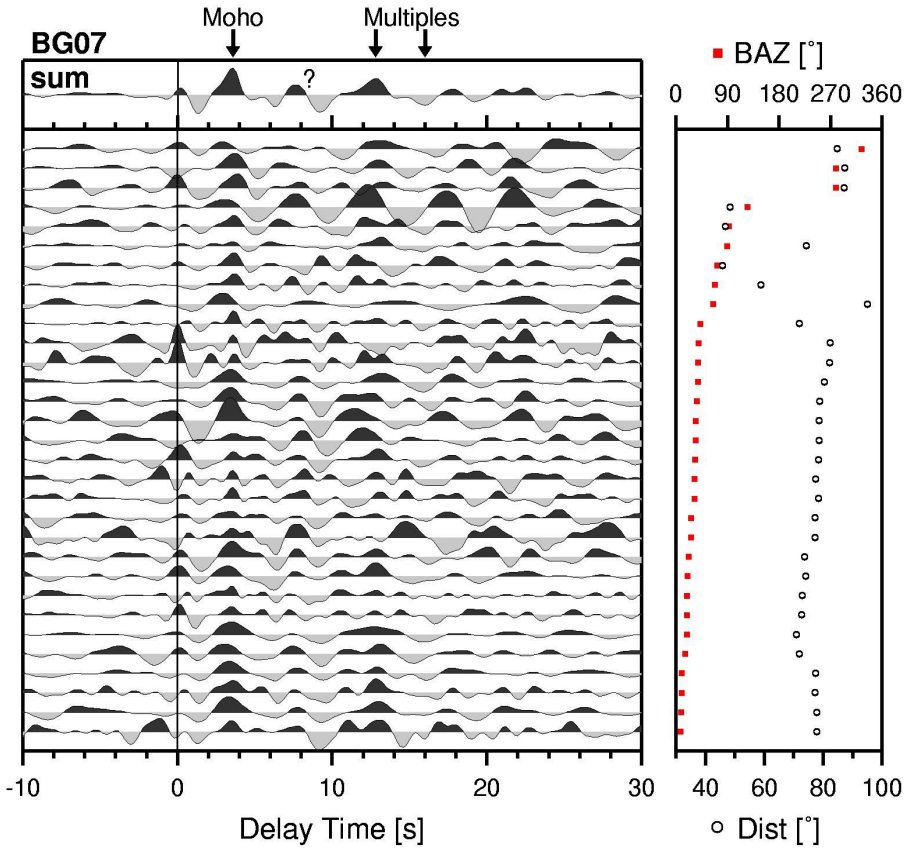
Moho
Multiples
BG07
sum
?
BAZ [°]
0 90 180 270 360
-10 0 10 20 30
Delay Time [s]
40 60 80 100
Dist [°]

e)

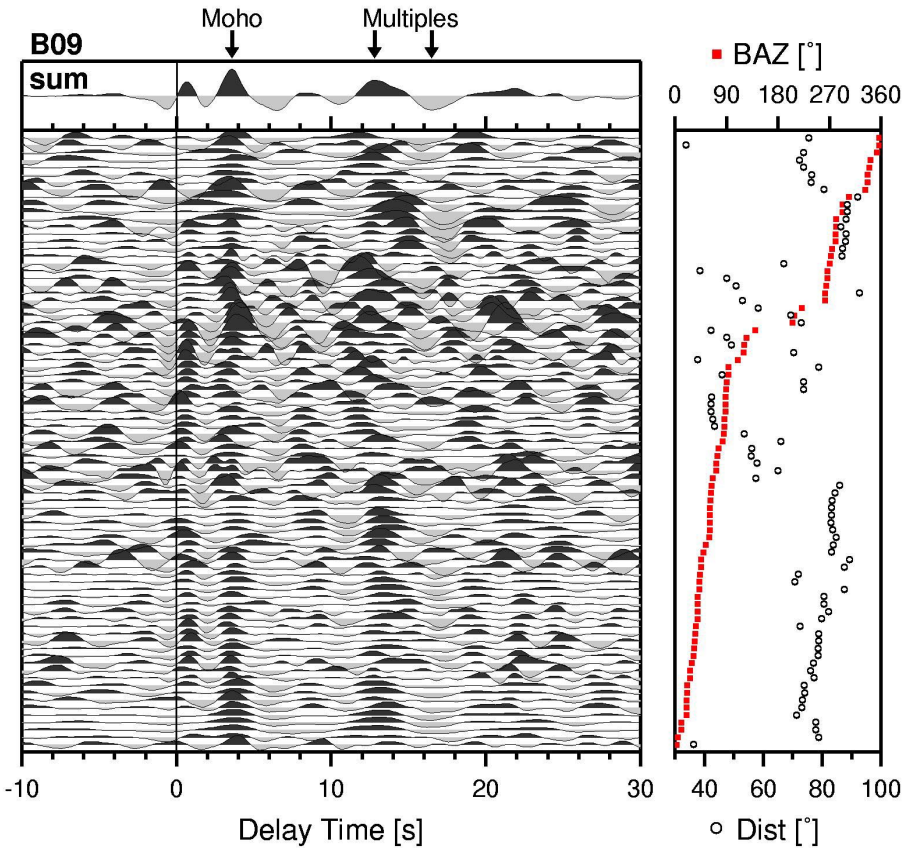
Moho
Multiples
B09
sum
BAZ [°]
0 90 180 270 360
-10 0 10 20 30
Delay Time [s]
40 60 80 100
Dist [°]

f)

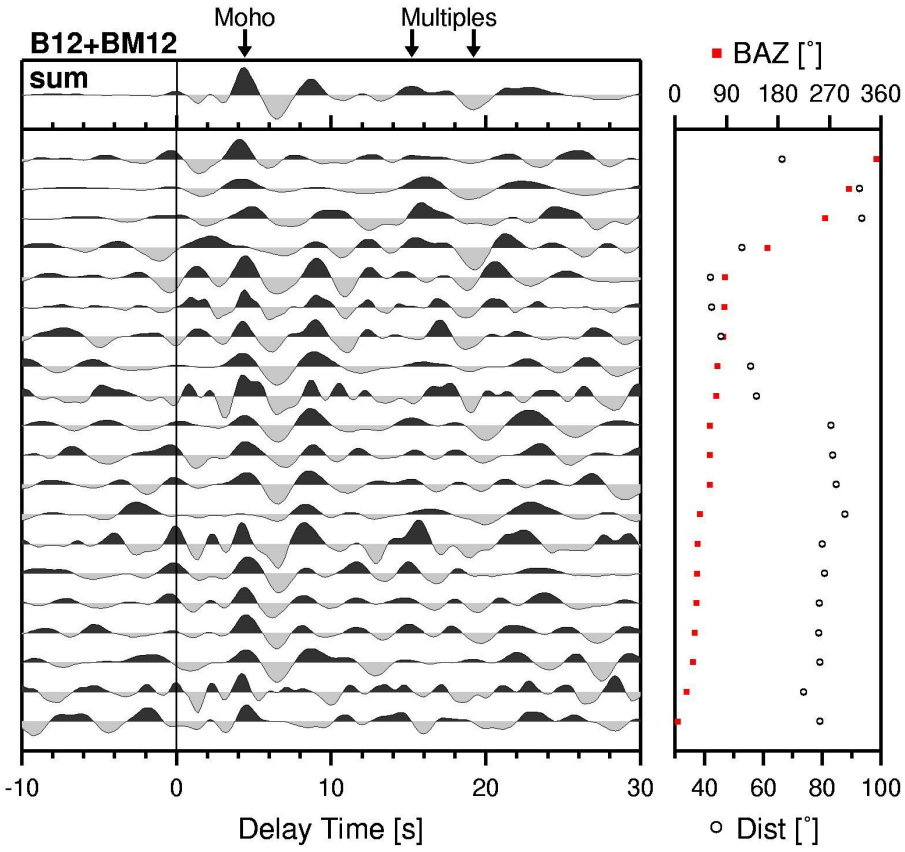
Moho
Multiples
B12+BM12
sum
BAZ [°]
0 90 180 270 360
-10 0 10 20 30
Delay Time [s]
40 60 80 100
Dist [°]

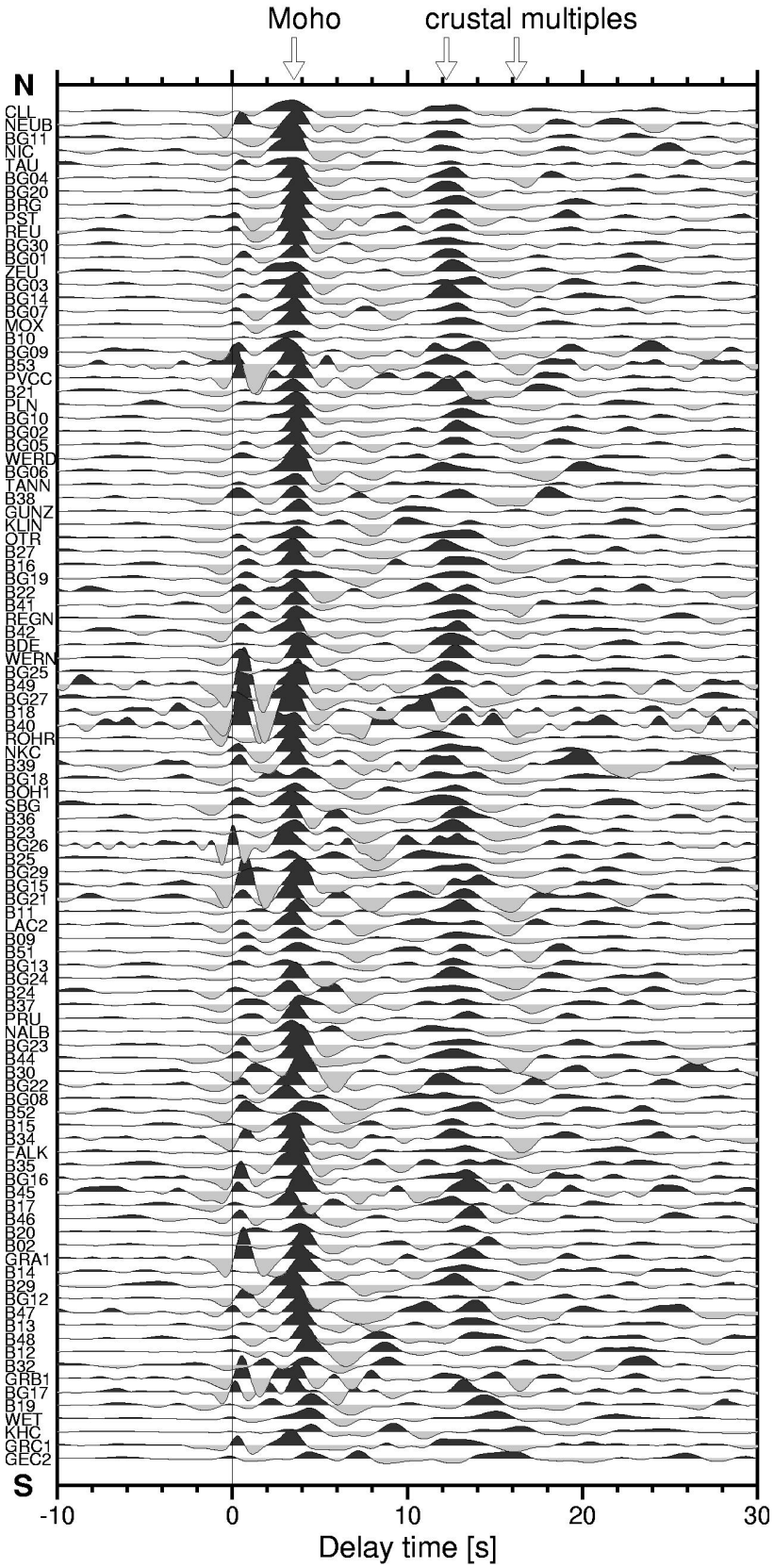

Figure 5.2: Sum traces of receiver functions of all stations of the BOHEMA passive seismic experiment that provided sufficient data for analysis. The time window between -10 and 30 s, which contains the conversion signal from the Moho discontinuity and crustal multiple reverberations is shown.

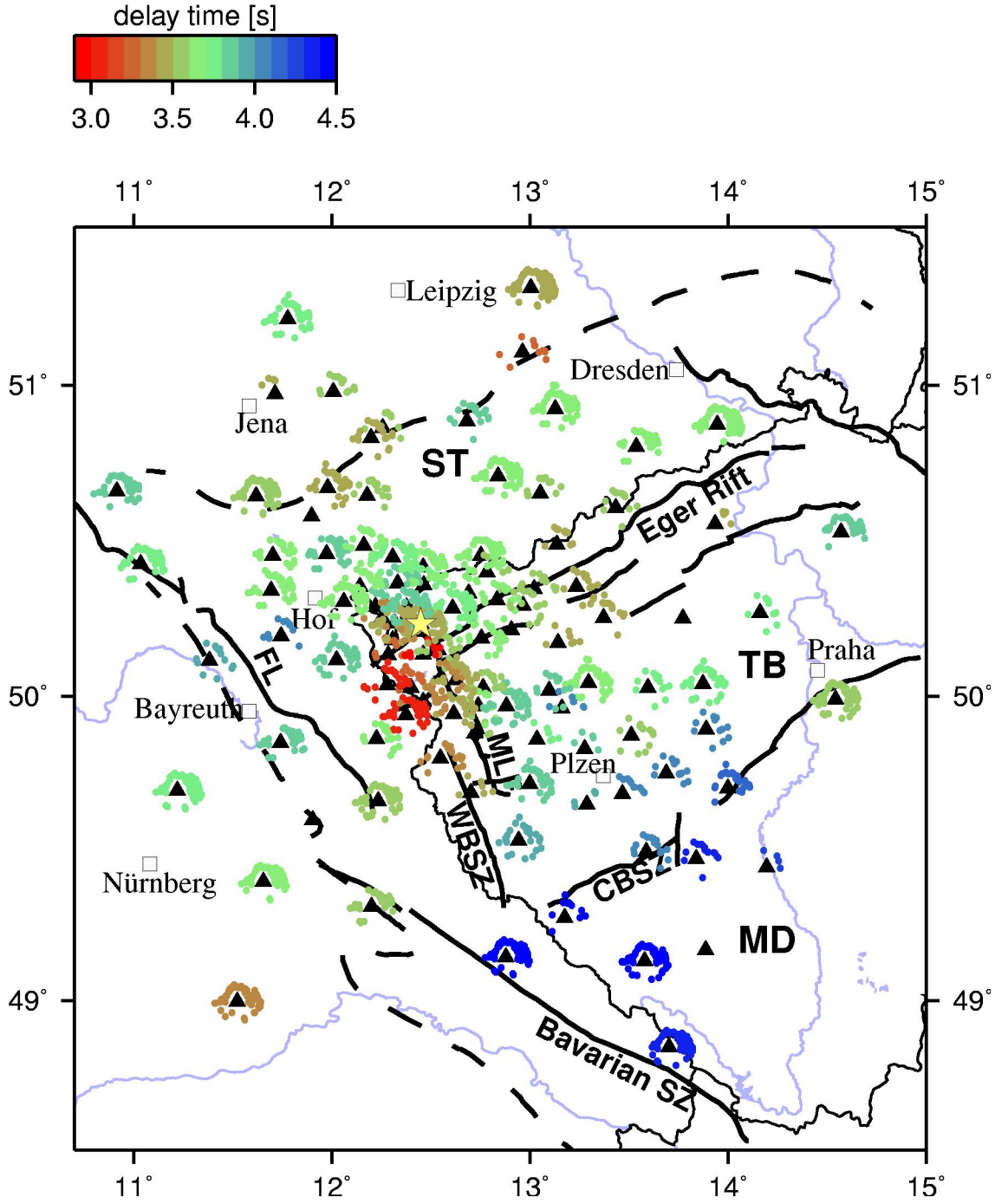

Figure 5.3: Delay times of the *Ps* conversion from the Moho discontinuity, obtained for stations of the BOHEMA experiment (more than 5000 receiver functions). Delay times vary between 3.0 and 4.5 s and are displayed together with the piercing points of the individual rays at 30 km depth. Stations without results for delay time either had not enough data or bad data quality. The yellow star marks the Nový Kostel main earthquake swarm area. For description of faults and tectonic units see Figure 3.1.

5.3.2 Crustal v_p/v_s ratios

In order to obtain the depth of the Moho discontinuity from the measured delay times of the *Ps* conversion, the method by *Zhu and Kanamori* (2000) was used to calculate average crustal v_p/v_s ratios for 34 BOHEMA stations with clear Moho *Ps* conversions and crustal multiples. The sum traces of these 34 stations are shown in Figure 5.4. For the inversion, an average crustal *P*-wave velocity of 6.3 km/s reported by *Hrubcová et al.* (2005) was used. From the obtained Moho depth and v_p/v_s values for each station, the delay time of the Moho *Ps* conversion and crustal multiples can be re-calculated to test the accuracy of the results. The re-calculated delay times are also shown in Figure 5.4. They generally agree very well with the measured delay times for all stations.

Examples of inversion results of Moho depth versus v_p/v_s are shown for temporary stations BG10 and BG24 in Figure 5.5. For the other stations, results of the inversion are shown in Appendix C.1. The 34 obtained v_p/v_s ratios are plotted into the map in Figure 5.6. The values vary between 1.66±0.06 (stations PRU, B17) and 1.81±0.08 (station BG25) with an average value of 1.73.

In the Saxothuringian unit, v_p/v_s ratios vary between 1.72 and 1.81 except for station PLN (1.67). In the Teplá-Barrandian unit, there seems to be a division into a northwestern part with values around 1.71 and a southeastern part (near the Central Bohemian Shear Zone) with values around 1.75.

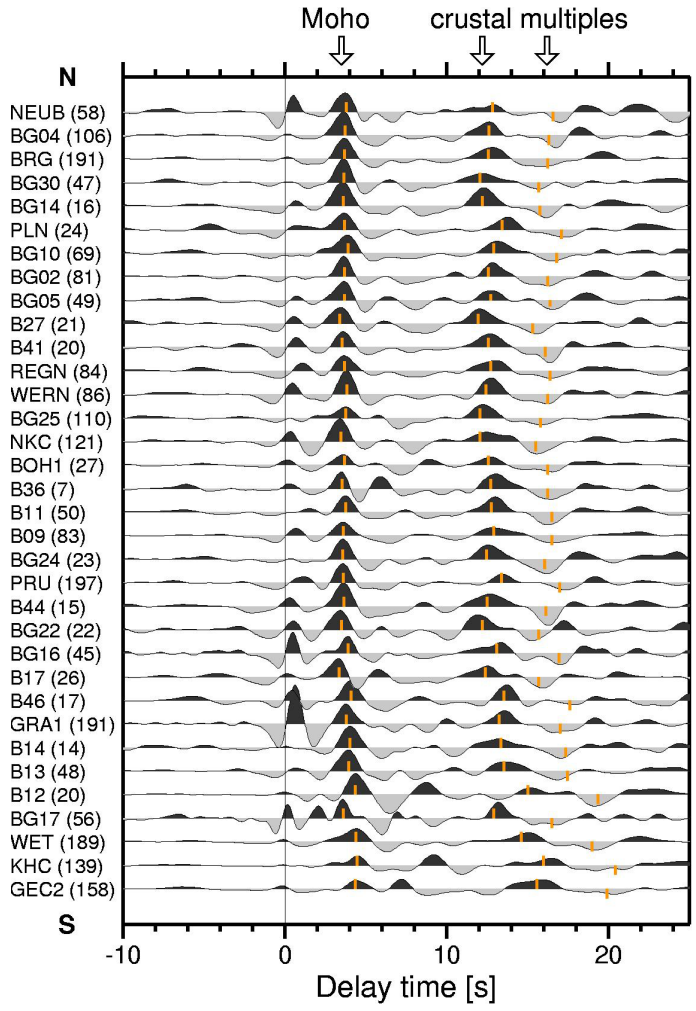

Figure 5.4: Sum traces of 34 BOHEMA stations with clear Moho *Ps* conversions and crustal multiples that were used for the grid search method by *Zhu and Kanamori* (2000). Stations are sorted from S (bottom) to N (top). Beside each trace, the name of the station and, in brackets, the number of individual traces used for stacking is given. For visual control of the results, the obtained values of Moho depth and v_p/v_s can be used to re-calculate the delay time of the Moho *Ps* conversion and the crustal multiples at each station. This is shown by the oranges dashes. The reproduced values agree very well with the data.

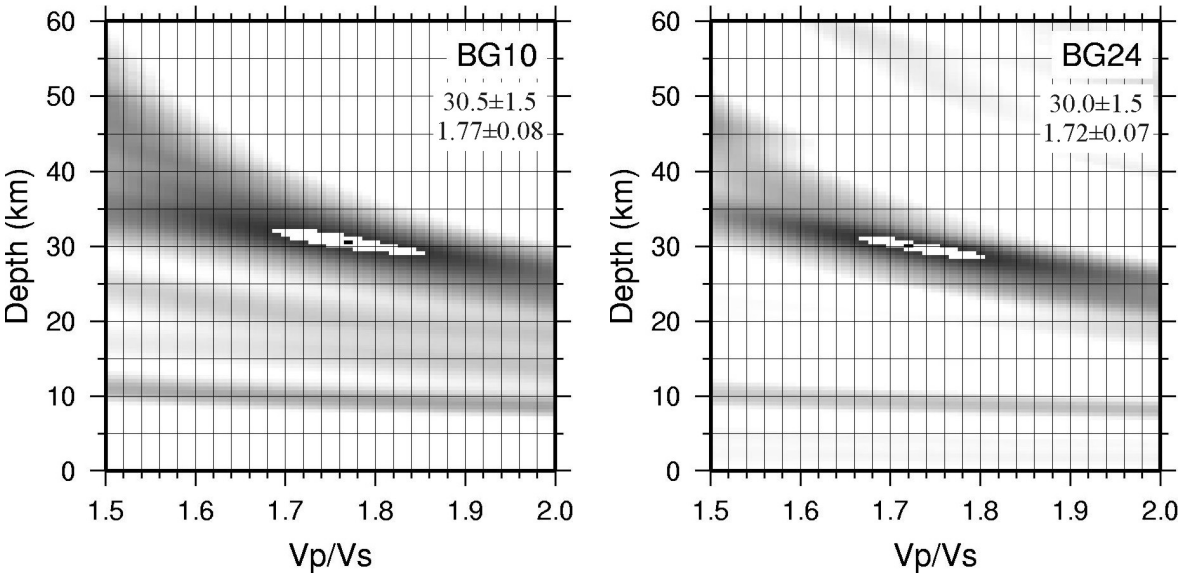

Figure 5.5: Depth of the Moho and v_p/v_s ratio obtained for stations BG10 and BG24 with the method by *Zhu and Kanamori* (2000). The grid search was carried out for an assumed average crustal *P*-wave velocity of 6.3 km/s in the intervals of 20 to 60 km for the Moho depth and 1.50 to 2.00 for v_p/v_s. The maximum stacked amplitude is marked by a black dot surrounded by a white ellipse. The latter one marks the area of 95% of the maximum stacked amplitude and thus gives an estimate of the uncertainty of the obtained values.

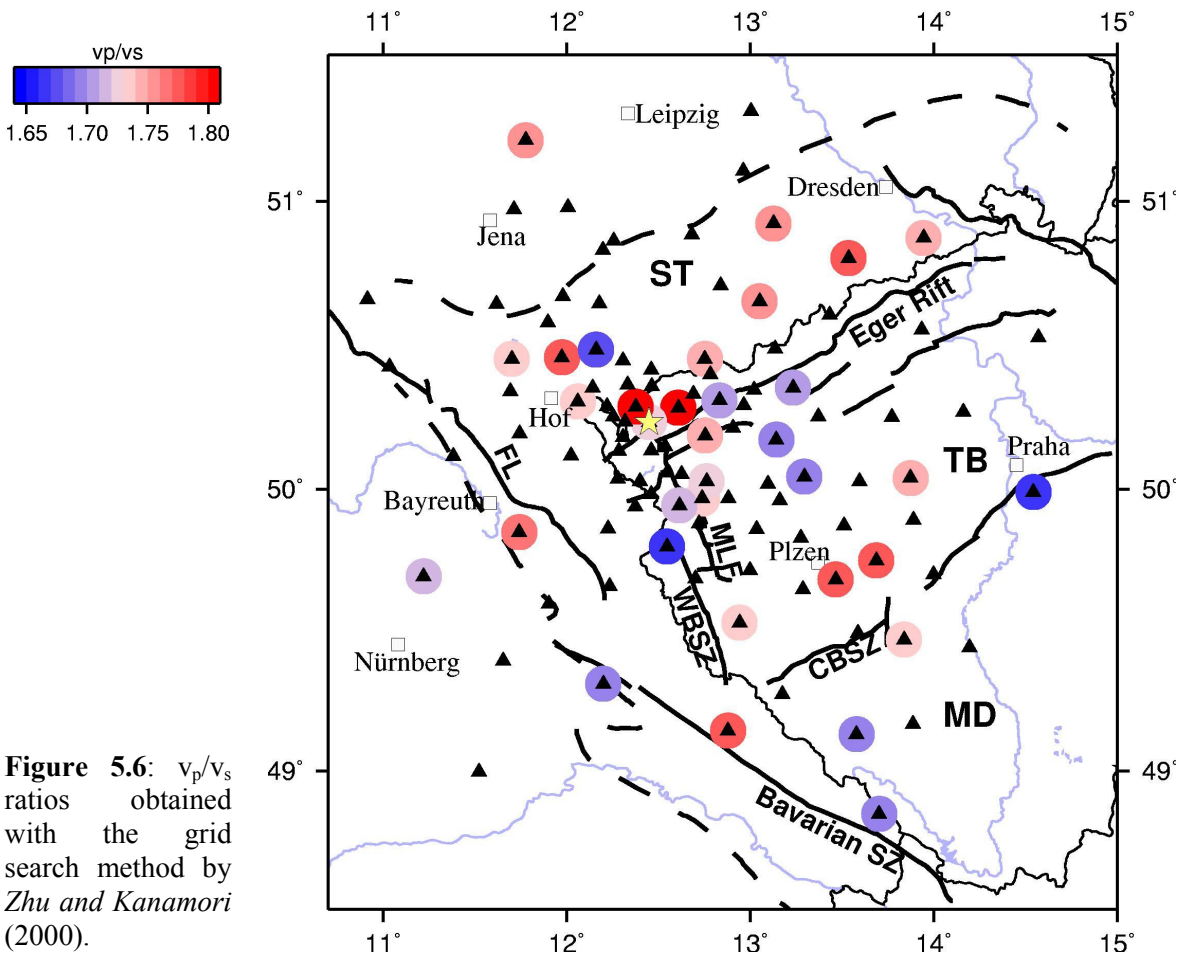

Figure 5.6: v_p/v_s ratios obtained with the grid search method by *Zhu and Kanamori* (2000).

5.4 Discussion

5.4.1 Map of crustal v_p/v_s ratios

In order to calculate Moho depths, v_p/v_s ratios must be provided for all stations. For 34 stations average crustal v_p/v_s ratios were obtained with the method of *Zhu and Kanamori* (2000). For the remaining stations, the investigated area was divided into subareas associated with the tectonometamorphic Variscan units of the Bohemian Massif. This step

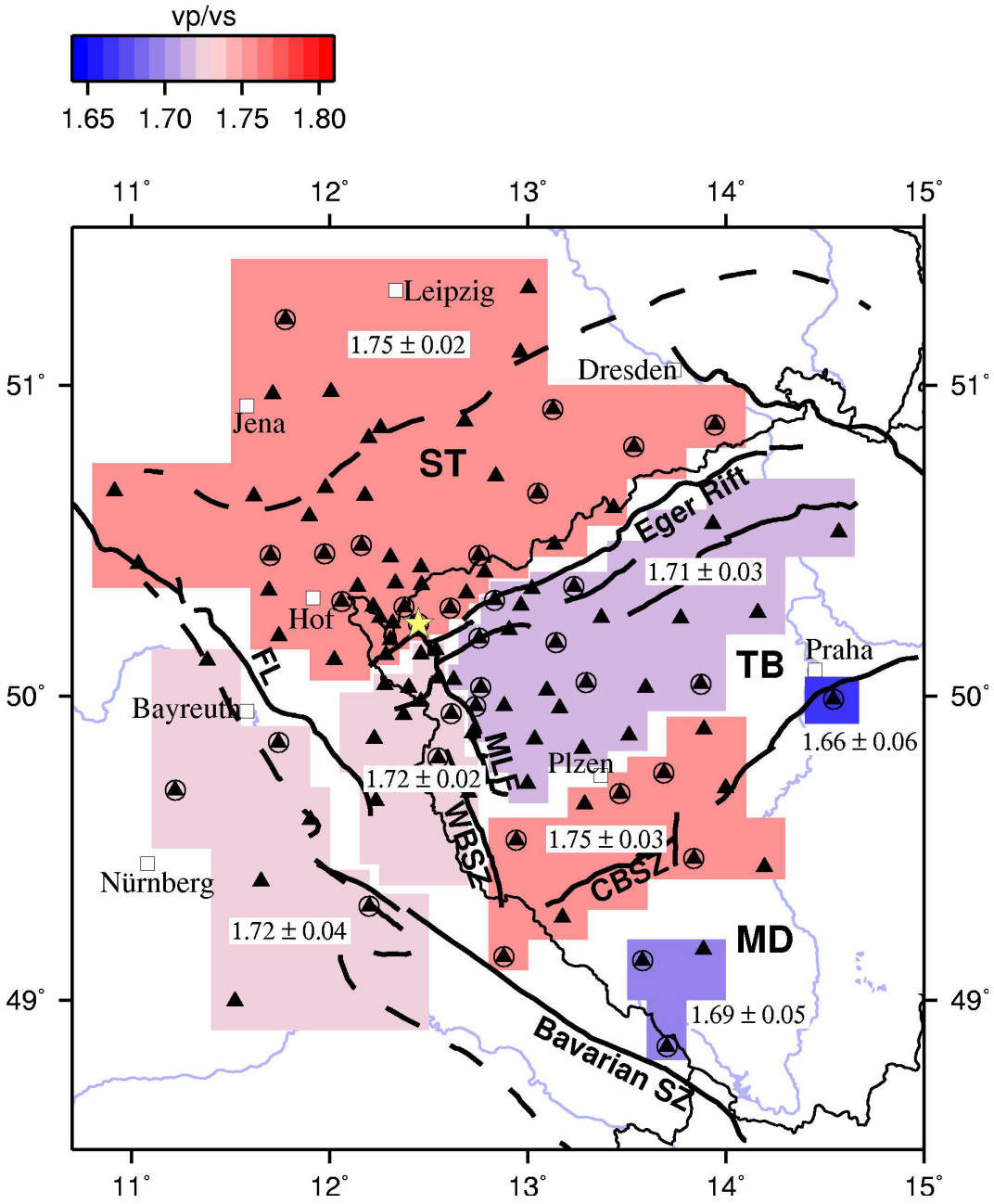

Figure 5.7: Division of the investigation area into subareas associated with the tectonometamorphic units of the Bohemian Massif. Mean v_p/v_s ratios and their standard deviations were calculated from the values obtained with the method by *Zhu and Kanamori* (2000) (Figure 5.6, Table 5.1).

is based on the simplifying assumption that the crust beneath each Variscan structural unit is more or less homogeneous. For the subareas, mean values of v_p/v_s ratios and their standard deviations were calculated of the values obtained with the method by *Zhu and Kanamori* (2000). The results are shown in Figure 5.7. The v_p/v_s ratios of all BOHEMA stations are summarized in Table 5.1.

In the resulting map (Figure 5.7), the Saxothuringian part of the Bohemian Massif displays a relatively high mean v_p/v_s ratio of 1.75±0.02. To the southeast, the northern part of the Teplá-Barrandian was combined to an area of a mean v_p/v_s ratio of 1.71±0.03. The transition of the Central Bohemian Shear Zone has a higher value again of 1.75±0.03. This corresponds to results by *Hrubcová et al.* (2005) who report a vp/vs ratio of 1.76 in the upper crust in the vicinity of the Central Bohemian Shear Zone. *Zhu and Kanamori* (2000) also report increased v_p/v_s ratios of more than 1.80 along a major shear zone (Eastern Californian Shear Zone, California). However, the West and North Bohemian Shear Zones do not show such a clear pattern. Station PRU near Prague stands alone with a rather low value of 1.66±0.06. In the Moldanubian unit southeast of the Central Bohemian Shear Zone, an area of low v_p/v_s ratio of 1.69±0.05 was obtained. Such low v_p/v_s ratios might for example be explained by quartz rich rocks beneath the stations (*Christensen*, 1996). In the Moldanubian region west of the Teplá-Barrandian unit, the mean v_p/v_s ratio is 1.72±0.02. As there are only two measured values in this rather large subarea, the mean value of each of the neighbouring subareas was included in the calculation. Hence, the standard deviation of this v_p/v_s ratio is also small. Finally, the region southwest of the Bohemian Massif which is covered by Mesozoic sediments, displays a mean v_p/v_s ratio of 1.72±0.04.

For some locations near the western Eger Rift and north of it, the v_p/v_s ratio changes rapidly over a short distance (e.g. stations BG10/PLN and BG25/B41, Figure 5.6). This could be caused by short-wavelength variation of crustal *P* and *S* velocities. It might also be an artefact due to the uncertainty of the v_p/v_s estimation (*Zhu and Kanamori*, 2000). These local differences are levelled out in the map of mean v_p/v_s ratios (Figure 5.7).

A comparison of v_p/v_s ratios obtained in the study by *Geissler et al.* (2005) and in this thesis at stations used in both investigations (Table 5.2) shows that most values agree very well within ± 0.02, except for station A02/PLN, where the difference is 0.05. Unfortunately, the estimated error of the v_p/v_s ratio is generally high. The crustal v_p/v_s ratio is so far among the least constrained parameters from both laboratory and field measurements.

The reason for the differences is that different teleseismic events and recording time spans were used in the two investigations.

High values of v_p/v_s beneath the western Erzgebirge mountains reported by *Geissler et al.* (2005) can partly be confirmed (stations WERN, BG25), the same is the case for reported low values at the Czech-German border east of KTB (station B17).

Table 5.1: Station parameters of BOHEMA stations (including station code, latitude and longitude), number of stacked receiver function traces (n), delay time of the Moho *Ps* conversion (t_{Ps}), v_p/v_s ratios and Moho depth H obtained with method by *Zhu and Kanamori* (2000), v_p/v_s ratios of the subareas (see Figure 5.7) and Moho depth H calculated either with the v_p/v_s ratios from inversion of Moho depth versus v_p/v_s or with v_p/v_s ratios of the related subareas

Station	Lat [°N]	Lon [°E]	n	t_{Ps} [s]	v_p/v_s (Z&K)	H [km] (Z&K)	v_p/v_s subarea	H [km]
B02	49.6992	13.996	51	4.10	-	-	1.75±0.03	33.0±2.0
B09	50.0422	13.2930	83	3.60	1.69±0.07	31.5±1.5	1.69±0.07	31.5±1.5
B10	50.6072	13.4315	16	3.50	-	-	1.75±0.02	28.5±2.0
B11/BM11	50.0382	13.8717	50	3.76	1.74±0.07	30.5±1.5	1.74±0.07	30.5±1.5
B12/BM12	49.4673	13.8379	20	4.40	1.73±0.05	36.0±1.5	1.73±0.05	36.0±1.5
B13/BM13	49.5285	12.9410	48	3.84	1.73±0.07	32.5±1.5	1.73±0.07	32.5±1.5
B14/BM14	49.6811	13.4646	14	3.80	1.77±0.07	31.5±1.5	1.77±0.07	31.5±1.5
B15/BM15	49.8718	13.5108	20	3.48	-	-	1.71±0.03	29.5±2.0
B16	50.3471	13.0187	18	3.52	-	-	1.71±0.03	30.0±2.0
B17	49.7965	12.5460	26	3.32	1.66±0.06	30.5±1.0	1.66±0.06	30.5±1.0
B18	50.252	13.3695	13	3.40	-	-	1.71±0.03	29.0±2.0
B19	49.2743	13.1726	13	4.50	-	-	1.75±0.03	36.5±2.0
B20	49.7126	12.9962	63	3.85	-	-	1.71±0.03	33.0±2.0
B21	50.4903	13.1356	13	3.44	-	-	1.75±0.02	28.0±2.0
B22	50.3326	12.6899	5	3.60	-	-	1.75±0.02	29.0±2.0
B23	50.1497	12.5365	22	3.52	-	-	1.72±0.02	29.5±2.0
B24	50.0264	12.3988	15	3.20	-	-	1.72±0.02	27.0±2.0
B25	50.1325	12.283	22	3.24	-	-	1.75±0.02	26.0±2.0
B27	50.3529	13.2317	21	3.44	1.70±0.10	29.0±1.5	1.70±0.10	29.0±1.5
B29	49.6845	12.7000	8	3.44	-	-	1.72±0.02	29.0±2.0
B30	49.959	13.160	8	4.00	-	-	1.71±0.03	34.0±2.0
B32	49.4393	14.1926	4	4.20	-	-	1.75±0.03	34.0±2.0
B33	49.168	13.886	1	-	-	-	1.69±0.05	-
B34	49.8776	12.7188	4	3.52	-	-	1.72±0.02	29.5±2.0
B35	49.8574	13.0340	8	3.76	-	-	1.71±0.03	32.0±2.0
B36	50.1729	13.1408	7	3.48	1.69±0.05	31.0±1.0	1.69±0.05	31.0±1.0
B37	50.0179	13.0945	17	3.84	-	-	1.71±0.03	32.5±2.0
B38	50.4003	12.7817	9	3.56	-	-	1.75±0.02	29.0±2.0
B39	50.2144	12.9050	3	3.64	-	-	1.71±0.03	31.0±2.0
B40	50.2513	13.7709	5	-	-	-	1.71±0.03	-
B41	50.3097	12.8324	20	3.60	1.70±0.07	30.5±1.5	1.70±0.07	30.5±1.5
B42	50.2917	12.9632	17	3.52	-	-	1.71±0.03	30.0±2.0
B44	49.9660	12.7365	15	3.60	1.73±0.07	30.0±1.5	1.73±0.07	30.0±1.5
B45	49.8266	13.2757	6	3.88	-	-	1.71±0.03	33.0±2.0
B46	49.7481	13.6850	17	4.04	1.77±0.06	32.0±1.0	1.77±0.06	32.0±1.0
B47	49.6457	13.2859	9	3.92	-	-	1.75±0.03	31.5±2.0
B48	49.4909	13.5845	19	4.08	-	-	1.75±0.03	33.0±2.0
B49	50.2696	14.1591	14	3.72	-	-	1.71±0.03	31.5±2.0
B51	50.0258	13.5951	17	3.72	-	-	1.71±0.03	31.5±2.0
B52	49.8909	13.8877	18	4.08	-	-	1.75±0.03	33.0±2.0
B53	50.5557	13.9331	4	3.44	-	-	1.71±0.03	29.5±2.0
BDE	50.2885	12.2198	13	3.80	-	-	1.75±0.02	30.5±2.0
BG01	50.7086	12.8369	141	3.64	-	-	1.75±0.02	29.5±2.0
BG02	50.4538	12.7407	81	3.64	1.74±0.06	30.0±1.0	1.74±0.06	30.0±1.0
BG03	50.6604	10.9144	54	3.80	-	-	1.75±0.02	30.5±2.0
BG04	50.9227	13.1249	106	3.62	1.75±0.06	30.0±1.0	1.75±0.06	30.0±1.0
BG05	50.4534	11.6998	49	3.64	1.73±0.07	30.5±1.5	1.73±0.07	30.5±1.5
BG06	50.4268	11.0356	66	3.72	-	-	1.75±0.02	30.0±2.0
BG07	50.6463	12.1766	31	3.56	-	-	1.75±0.02	29.0±2.0
BG08	49.9380	12.3729	82	3.08	-	-	1.72±0.02	26.0±2.0

continued on next page

Station	Lat [°N]	Lon [°E]	n	t_{Ps} [s]	v_p/v_s (Z&K)	H [km] (Z&K)	v_p/v_s subarea	H [km]
BG09	50.5814	11.8954	19	3.04	-	-	1.75±0.02	24.5±2.0
BG10	50.4589	11.9729	69	3.84	1.77±0.08	30.5±1.5	1.77±0.08	30.5±1.5
BG11	51.1030	12.9620	13	3.28	-	-	1.75±0.02	26.5±2.0
BG12	49.6573	12.2322	115	3.56	-	-	1.72±0.02	30.0±2.0
BG13	50.0346	12.2787	36	3.02	-	-	1.72±0.02	25.5±2.0
BG14	50.6534	13.0504	16	3.56	1.75±0.07	29.0±1.5	1.75±0.07	29.0±1.5
BG15	50.1147	11.3821	20	3.92	-	-	1.72±0.04	33.0±2.0
BG16	49.8468	11.7405	45	3.88	1.76±0.05	31.0±1.0	1.76±0.05	31.0±1.0
BG17	49.3096	12.1983	56	3.56	1.69±0.04	31.5±1.0	1.69±0.04	31.5±1.0
BG18	50.1938	11.7432	12	(4.08?)	-	-	1.75±0.02	-
BG19	50.3408	11.6928	62	3.60	-	-	1.75±0.02	29.0±2.0
BG20	50.8852	12.6796	31	3.80	-	-	1.75±0.02	30.5±2.0
BG21	50.0576	12.5476	16	3.36	-	-	1.72±0.02	28.0±2.0
BG22	49.9416	12.6133	22	3.40	1.71±0.06	29.5±1.0	1.71±0.06	29.5±1.0
BG23	49.9668	12.8785	79	3.84	-	-	1.71±0.03	32.5±2.0
BG24	50.0270	12.7614	23	3.58	1.72±0.07	30.0±1.5	1.72±0.07	30.0±1.5
BG25	50.2833	12.6068	110	3.74	1.81±0.08	28.0±1.5	1.81±0.08	28.0±1.5
BG26	50.1336	12.4583	12	2.96	-	-	1.72±0.02	25.0±2.0
BG27	50.2531	12.2525	9	3.36	-	-	1.75±0.02	27.0±2.0
BG28	49.5947	11.9037	20	?	-	-	1.72±0.04	-
BG29	50.1171	12.0219	60	3.88	-	-	1.75±0.02	31.5±2.0
BG30	50.8035	13.5353	47	3.60	1.77±0.06	28.5±1.0	1.77±0.06	28.5±1.0
BOH1	50.1866	12.7538	27	3.60	1.74±0.06	30.0±1.0	1.74±0.06	30.0±1.0
BRG	50.8732	13.9428	191	3.64	1.74±0.07	30.0±1.5	1.74±0.07	30.0±1.5
CLL	51.3077	13.0026	187	3.44	-	-	1.75±0.02	28.0±2.0
FALK	49.8597	12.2236	27	3.60	-	-	1.72±0.02	30.5±2.0
GEC2	48.8451	13.7016	158	4.36	1.69±0.07	38.0±1.75	1.69±0.07	38.0±1.75
GRA1	49.6910	11.2200	191	3.76	1.71±0.06	32.0±1.5	1.71±0.06	32.0±1.5
GRB1	49.3920	11.6540	175	3.68	-	-	1.72±0.04	31.0±2.0
GRC1	48.9960	11.5220	181	3.36	-	-	1.72±0.04	28.0±2.0
GUNZ	50.3635	12.3316	43	3.80	-	-	1.75±0.02	30.5±2.0
KHC	49.1309	13.5782	139	4.48	1.69±0.06	39.0±1.5	1.69±0.06	39.0±1.5
KLIN	50.3584	12.4616	20	(3.76?)	-	-	1.75±0.02	(30.5?)
LAC2	50.0508	12.6250	47	3.40	-	-	1.71±0.03	29.0±2.0
MOX	50.6447	11.6156	176	3.56	-	-	1.75±0.02	29.0±2.0
NALB	49.9812	12.4607	21	3.36	-	-	1.72±0.02	28.0±2.0
NEUB	51.2085	11.7755	58	3.72	1.75±0.07	30.5±1.0	1.75±0.07	30.5±1.0
NIC	50.9782	12.0047	18	3.56	-	-	1.75±0.02	29.0±2.0
NKC	50.2331	12.4479	121	3.40	1.72±0.08	29.0±1.5	1.72±0.08	29.0±1.5
OTR	50.3531	12.1388	30	3.68	-	-	1.75±0.02	29.5±2.0
PLN	50.4860	12.1590	24	3.64	1.67±0.06	33.0±1.5	1.67±0.06	33.0±1.5
PRU	49.9883	14.5417	197	3.56	1.66±0.06	33.0±1.5	1.66±0.06	33.0±1.5
PST	50.8640	12.2550	10	3.56	-	-	1.75±0.02	29.0±2.0
PVCC	50.5282	14.5690	65	3.88	-	-	1.71±0.03	33.0±2.0
REGN	50.3060	12.0606	84	3.64	1.73±0.08	30.5±1.5	1.73±0.08	30.5±1.5
REU	50.8310	12.1960	26	3.44	-	-	1.75±0.02	28.0±2.0
ROHR	50.2346	12.3168	99	3.44	-	-	1.75±0.02	28.0±2.0
SBG	50.1820	12.3050	4	(3.36)	-	-	1.75±0.02	-
TANN	50.4160	12.4600	81	3.60	-	-	1.75±0.02	29.0±2.0
TAU	50.9716	11.7111	6	(3.44)	-	-	1.75±0.02	-
WERD	50.4480	12.3070	55	3.72	-	-	1.75±0.02	30.0±2.0
WERN	50.2874	12.3761	86	3.80	1.80±0.08	29.0±1.0	1.80±0.08	29.0±1.0
WET	49.1440	12.8782	189	4.40	1.77±0.08	34.5±2.0	1.77±0.08	34.5±2.0
ZEU	50.6719	11.9780	43	3.40	-	-	1.75±0.02	27.5±2.0

Table 5.2: Comparison of v_p/v_s ratios obtained in the study by *Geissler et al.* (2005) and in this thesis at stations used in both investigations. In both studies, the values were obtained with the method by *Zhu and Kanamori* (2000). The last column gives the mean v_p/v_s ratio of the subarea in which the station is located (see Figure 5.7). Differences of the values are caused by different recording time spans of teleseismic events in the two investigations.

Station	v_p/v_s (Geissler et al., 2005)	v_p/v_s (this study)	mean v_p/v_s subarea
A02/PLN	1.72±0.08	1.67±0.06	1.75±0.02
A21/REGN	1.74±0.07	1.73±0.08	1.75±0.02
BRG	1.76±0.08	1.74±0.07	1.75±0.02
GRA1	1.73±0.05	1.71±0.06	1.72±0.04
KHC	1.71±0.05	1.69±0.06	1.69±0.05
NKC	1.73±0.07	1.72±0.08	1.75±0.02
WER/WERN	1.79±0.08	1.80±0.08	1.75±0.02
WET	1.79±0.09	1.77±0.08	1.75±0.03

5.4.2 Depth map of the Moho discontinuity

The Moho depth at each station was calculated using the *Ps* delay time, v_p/v_s ratio and an average crustal *P* wave velocity of 6.3 km/s (Figure 5.8, Table 5.1) (*Heuer et al.*, 2006). A smoothed map of Moho depths of the central part of the investigated area is given in Figure 5.9. The Moho depth values have an estimated uncertainty of ±2 km. They were not corrected for topography as topography is relatively small compared to the resolution of the method (see Appendix A.1, altitudes of seismic stations).

Crustal thicknesses display values of 27 to 31 km in the Saxothuringian unit (except for station PLN due to the very low v_p/v_s ratio), 30 to 33 km in the Teplá-Barrandian and 34 to 39 km in the Moldanubian unit east of the Bavarian Shear Zone. Like in the map of delay times of the Moho *Ps* conversions (Figure 5.5), a prominent feature in the Moho depth map is an area of thin crust of about 26 to 28 km beneath the western Eger Rift. The internal geometry of this updoming seems to be irregular: towards the ENE, the crustal thickness gradually increases to „normal“ values of about 31 km, whereas towards the WSW there seems to be an abrupt depth increase from 26 to 31 km. This apparent Moho updoming was already observed with less resolution by *Geissler et al.* (2005). It corresponds well with the area of CO_2 degassing fields at surface. The main swarm earthquake area of Nový Kostel is situated at the northeastern margin of the Moho updoming area. The Moho depth increases towards the SE and reaches values of almost 40 km between the Central Bohemian and the Bavarian Shear Zone. This result is in good agreement with former seismic studies (e.g. *Hrubcová et al.*, 2005).

At the stations of the German Regional Seismic Network (GRSN) and GRF array in the investigation area, the depth of the Moho has been investigated in previous studies with the receiver function method (*Kind et al.*, 1995; *Wilde- Piórko et al.*, 2005; *Geissler et al.*, 2005). Some of the obtained depth values are compared with values obtained in the present study in Table 5.3. They agree very well with each other. Like in the present study, *Wilde-Piórko et al.* (2005) also find a thick crust of 35-40 km in the southeast, while the crust in the northwestern (Saxothuringian) part is much thinner (28-32 km).

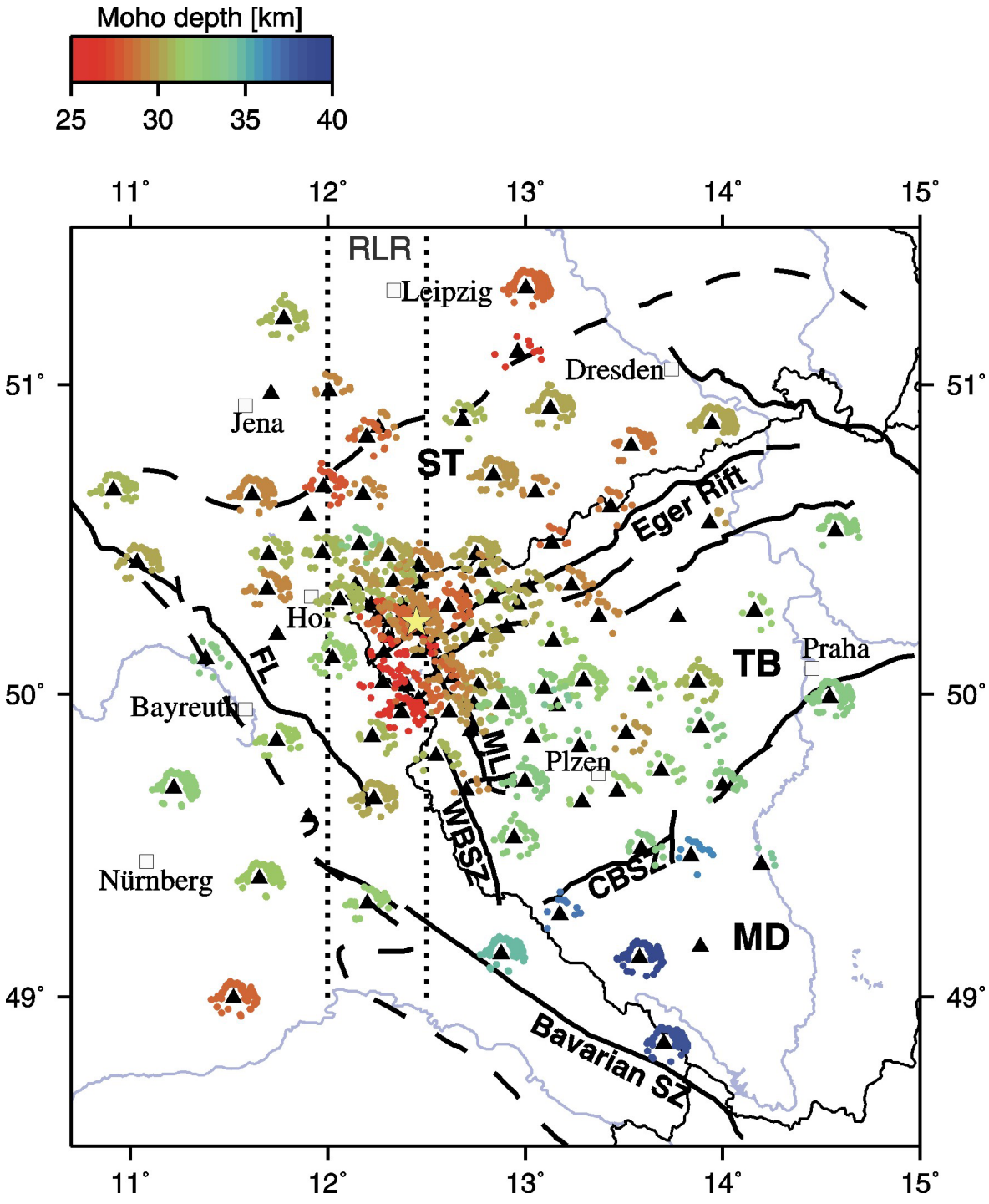

Figure 5.8: Moho depth values of each station were plotted at the piercing points of the individual rays at an interface at 30 km depth.

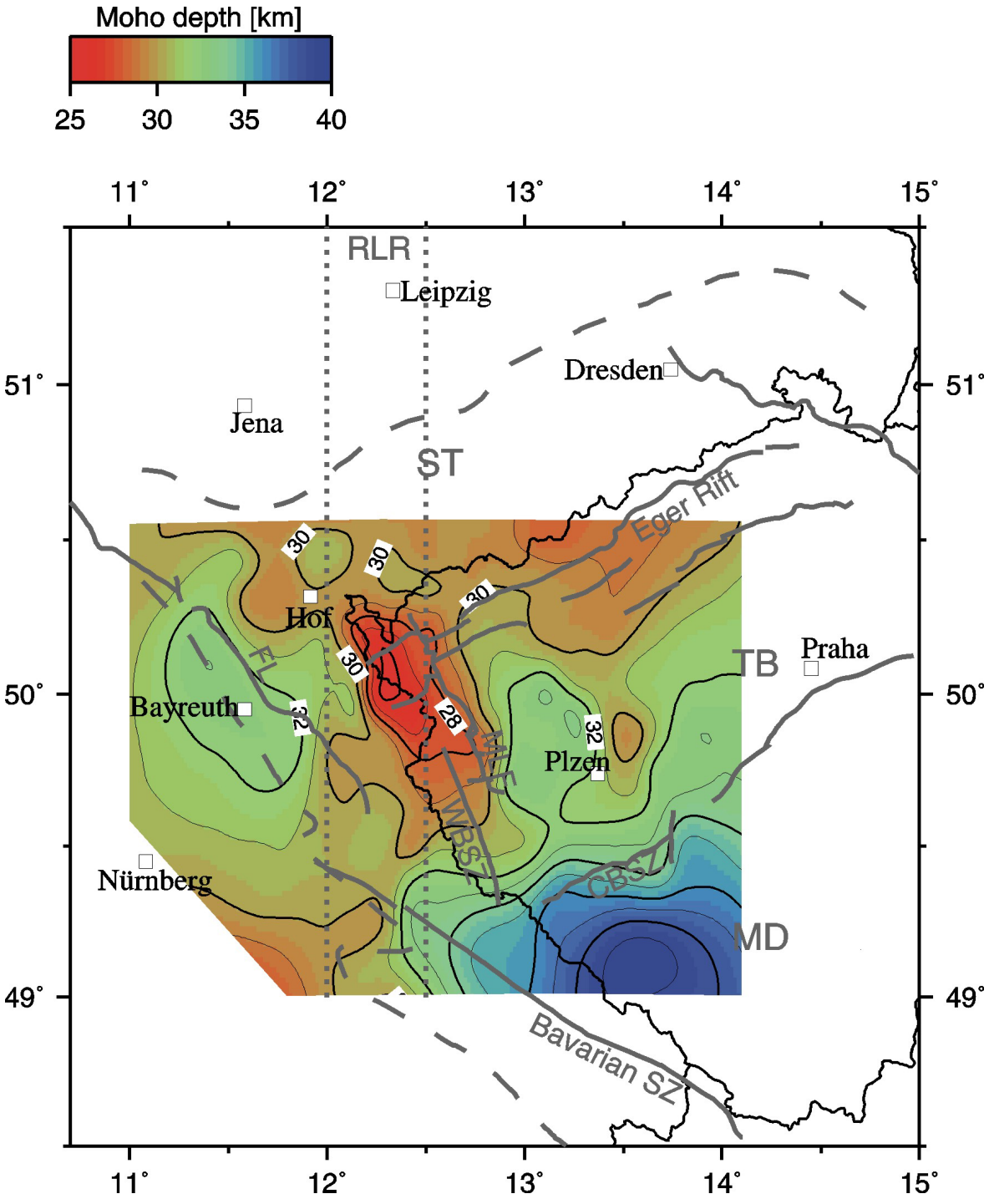

Figure 5.9: Simplified Moho depth map of the central part of the investigation area. The margins of the investigation area were cut off because boundary effects distort the proportions of the isothickness lines. Spacing of the thick lines is 2 km and of thin lines 1 km. The shading of colours is given in steps of 0.5 km.

Table 5.3: Moho depth values obtained in previous receiver function investigations at stations within and around the Bohemian Massif, compared to values of this thesis. RF means receiver function, Z&K means inversion by the grid search method of *Zhu and Kanamori* (2000).

Station	Moho depth [km]					
		Wilde-Piórko et al., 2005			*Geissler et al.*, 2005	*this study*
	Kind et al., 1995 (RF inversion)	RF inversion	RF forward	grid search (*Z&K*)	(Z&K)	(Z&K)
BRG	-	31.5±1.5	32.0±1.0	29.6±2.0	29.3±1.8	30.0±1.5
CLL	-	29.5±1.5	30.0±1.0	28.2±2.0	29.5±2.0	28.0±2.0
MOX	-	29.5±1.5	29.0±1.0	30.6±2.1	30.3±1.8	29.0±2.0
GRA1	32	-	-	-	31.5±0.5	32.0±1.5
GRB1	?	-	-	-	29.8±1.3	31.0±2.0
GRC1	?	-	-	-	30.3±1.8	28.0±2.0
WET	32	34.5±1.5	39.0±2.0	34.4±2.5	34.3±1.8	34.5±2.0
KHC	-	39.5±1.5	39.0±1.0	38.2±2.3	38.3±1.5	39.0±1.5
NKC	-	31.5±1.5	30.0±1.0	28.6±2.1	28.8±1.8	29.0±1.5
PRU	-	33.5±1.5	33.0±2.0	33.2±1.6	33.0±1.0	33.0±1.5

5.4.3 Comparison with seismic refraction profile CEL09

In the Saxothuringian unit, Moho depth generally varies between 27 and 31 km according to the data of this study. This is partly in contradiction to the interpretation of refraction seismic data by *Hrubcová et al.* (2005). They derived a strongly laminated lower crust in the Saxothuringian and partly the Teplá-Barrandian unit with an upper boundary at 25 to 27 km depth and a very gradual Moho as lower boundary at 34 to 35 km depth (see Figure 2.3 in Chapter 2). The Moho updoming observed in this thesis could correspond to the upper boundary of *Hrubcová et al.*'s lower crustal layer (*Heuer et al.*, 2006). Former seismic studies in the Saxothuringian also report a reflective lower crust which appears to be strongly laminated (*DEKORP Research Group,* 1985; *Behr and Heinrichs*, 1987; *DEKORP Research Group*, 1994; *Enderle et al.*, 1998). However, in the receiver function data presented here, an additional layer in the Saxothuringian unit can generally not be observed. Data of stations of the BOHEMA data set located close to the refraction seismic profile CEL09 are shown in Figure 5.10. They do not display indications of a second layer at lower crustal or Moho depth. If there were such a layer, the crustal multiple reflections should split into two phases and thus resolve a two-layered structure. However, one station (BG09) shows indications of an additional layer: the "Moho" *Ps* converted signal has a very short delay time corresponding to 24.5 km depth, which might as well be interpreted as a strong velocity contrast at the top of a lower crustal layer. And, more importantly, the multiple reverberations show a clear splitting into two peaks (Figure 5.10). Yet the neighbouring stations of BG09 do not show indications for a distinct lower crustal layer.

A comparable case is described by *Mohsen et al.* (2005), who observed a splitting of the multiples into two phases east of the Dead Sea Transform, while the Moho *Ps* conversion did not show indications for an additional layer. However, while steep angle reflections and receiver functions revealed this additional discontinuity in the lower crust, refraction

seismic data did not display this feature (*Mechie et al.*, 2005) –opposite than in this thesis and the refractions seismic experiment CEL09.

The apparent mismatch may have its origin in (1) different resolution scales of the two methods and (2) the complex nature of the crust mantle boundary in the area under investigation, possibly leading to the existence of two Mohos - a "refraction Moho" and a "RF Moho" (*Heuer et al.*, 2006).

Hrubcová et al. (2005) find that the Moldanubian is characterized by the deepest (39 km) and the most pronounced Moho within the whole Bohemian Massif with a strong velocity contrast, which agrees with the results of this thesis and other seismic studies (e.g. *Geissler et al.*, 2005; *Wilde- Piórko et al.,* 2005).

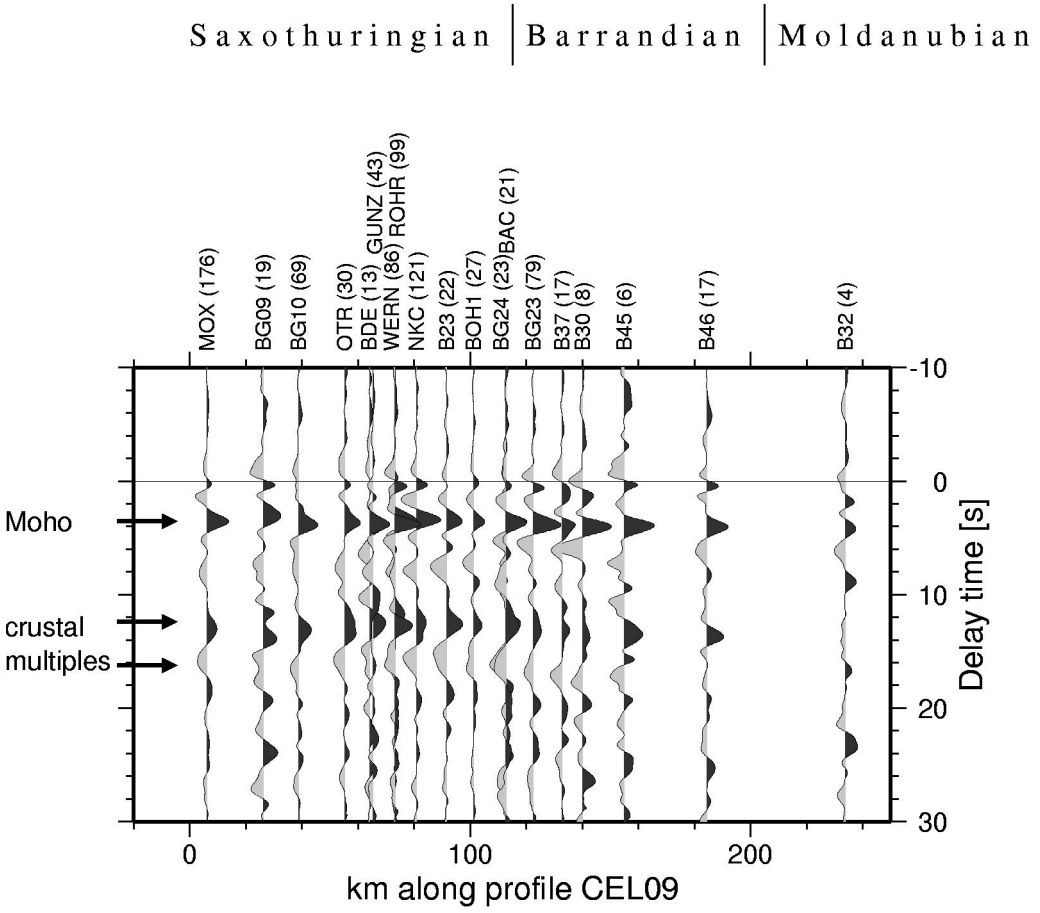

Figure 5.10: Sum traces of receiver functions at BOHEMA stations within 8 km distance from profile CEL09 (*Hrubcová et al.,* 2005). In the Saxothuringian unit, *Hrubcová et al.,* 2005 interpret a strong discontinuity at the top of the lower crust at 25 to 27 km depth and a very gradual Moho as lower boundary at 34 to 35 km depth. Except for station BG09, the receiver functions of the BOHEMA experiment show no indications for an additional discontinuity. In the receiver functions, Moho depth for the displayed stations varies around 29 to 30 km, except for station BG09 (24.5 km) which does not seem to fit to the neighbouring stations and might be an indication for strong discontinuity at the top of a lower crustal layer.